Chemotherapeutic drug delivery to cancer cells using a combination of folate targeting and tumor microenvironment-sensitive polypeptides

Wei Gao [a], Bai Xiang [a], Ting-Ting Meng [a], Feng Liu [b], Xian-Rong Qi [a,*]

[a] State Key Laboratory of Natural and Biomimetic Drugs, School of Pharmaceutical Sciences, Peking University, 38 Xueyuan Road, Beijing 100191, PR China
[b] Division of Molecular Pharmaceutics, School of Pharmacy, University of North Carolina, Chapel Hill, NC 27599-7360, USA

ARTICLE INFO

ABSTRACT

Chemotherapeutic agents often cause severe side effects because they produce a similar cytotoxicity in both cancerous and healthy cells. In this study, a rational strategy was implemented to take advantage of a combination of both tumor microenvironment-sensitive polypeptides (TMSP) and folate to create a more selective and efficient drug delivery system to target cancer cells. TMSP and folate were conjugated to the distal ends of DSPE-PEG$_{2000}$-maleimide and DSPE-PEG$_{5000}$-amine to create DSPE-PEG$_{2000}$-TMSP and DSPE-PEG$_{5000}$-folate, respectively, which were incorporated onto the surface of a docetaxel-loaded nanostructured lipid carrier (F/TMSP-DTX-NLC). TMSP are comprised of polycationic cell-penetrating peptides (CPP) and polyanionic inhibitory peptides, which are coupled via a proteinase-sensitive cleavable linker. The linker can be cleaved in the presence of matrix metalloprotease-2 and -9 (MMP-2/9). TMSP provides the ability to enhance specific cancer cellular uptake after selectively unmasking polyanionic inhibitory peptides in MMP-2/9 protease-oversecretion tumor tissue, whereas in circulation, the penetration is shielded. The folate moiety binds selectively to folate receptor-positive tumors. The cleaved dual-modified nanocarriers are then taken up by the tumor cells via both receptor-mediated endocytosis and CPP penetrating action to overcome the higher interstitial pressure in the tumor. The nanocarrier system demonstrated a small size, high encapsulation efficiency (>95%), sustained release and targeted delivery. The strong cellular uptake and cytotoxic activity of dual-modified F/TMSP-DTX-NLC in KB, HT-1080, MCF-7 and A549 cells verified the correlation with folate receptor expression and MMP-2/9 secretion. The remarkable penetration into KB and HT-1080 multicellular tumor spheroids confirmed that the temporary mask of the polyanionic inhibitory peptide in TMSP does not disturb the penetration ability of CPP in the tumor microenvironment with abundant proteases. Furthermore, the active targeting and triggered activation exhibited higher antitumor efficacy and lower systemic toxicity with the KB tumor model in nude mice compared to the nonmodified DTX–NLC and Taxotere®. These results suggested that the application of combined TMSP and folate modifications may be an approach in the selectively targeted delivery of anticancer drugs with low systemic toxicity.

1. Introduction

Several conventional nanocarriers (*e.g.*, liposomes, drug–polymer conjugates, polymeric nanoparticles and polymeric micelles) have been drawn significant attention to the delivery of chemotherapeutic drugs to targeted sites [1–5]. These nanocarrier systems accumulated in the tumor tissue via a passive targeting mechanism termed the enhanced permeability and retention (EPR) effect [6]. However, several intrinsic limitations in these delivery systems have become apparent due to their lack of specificity. To overcome these limitations such as the delivery of chemotherapeutic drugs to the desired sites at the appropriate time, a variety of approaches have been adopted. Tumor microenvironment-sensitive nanocarriers that respond to changes in environmental conditions such as pH, temperature, light, chemicals, biomolecules and electromagnetic fields have received extensive attention for their unique advantages in applications for target drug delivery.

The local tumor microenvironment notably enriched with a broad spectrum of proteases differs greatly from normal tissues.

The enzyme-sensitive substrate strategy is explorative and utilizes the stimulation of the unique proteases in the tumor environment based on the principle of proteolysis. Proteolysis is a simple hydrolytic process that separates two adjacent amino acid residues at the amide bond, which is triggered by proteases [7]. Because proteases are upregulated during disease progression, proteolysis has been proposed as a unique process to assist in therapy and diagnosis. Numerous approaches based on proteolysis have been crafted to manage diseases; for example, prodrugs have been designed to be activated by proteases, delivery systems have been constructed to release drugs in a controllable manner, and protease-sensitive molecular reporters have been prepared for disease detection and imaging [7–12].

The proteolytic specificities of peptide substrates provide modular chemical tools for the rational design of cell selectively permeable nanocarriers that are post-specifically activated by extracellular proteases present in the tumor tissues. MMP-2/9 are cell-surface, Zn-dependent endoproteases associated with diverse processes throughout tumor formation and progression, which play a critical role in tumor progression, angiogenesis, invasion and metastasis [9]. MMP-2/9 have become two of the most frequently used cleavable enzymes associated with cancer for targeted delivery systems [13]. Active targeting of nanocarriers in the tumor extracellular microenvironment, containing TMSP, mainly takes advantage of the selectivity and specificity of enzymes and enhances availability of the drug to tumors, therefore, significantly reduces toxicity to normal cells has been developed in our previous study [14].

The introduction of various biological ligands or antibodies into drug delivery systems has provided the opportunity for the selective delivery of drugs to tumor cells. Such ligands are recognized by specific receptors on certain types of cancer cell surfaces, which then induce the cellular uptake of the ligand-decorated carriers via receptor-mediated endocytosis [15]. Among cancer-specific ligands, folate, a small-molecule targeting ligand, has a high affinity ($K_d \sim$ 0.1–1 nmol/L) for the folate receptor (FR), which has been widely employed as a targeting moiety for various anticancer drugs and nanocarriers [16,17]. FR is a 38 kDa glycosyl phosphatidylinositol-anchored protein overexpressed by many primary and metastatic cancers, including ovarian and breast cancers, while its expression is highly restricted in normal cells [18–21].

In this study, a rational strategy was employed to take advantage of a combination of both TMSP and folate to create a more selective and efficient drug delivery system to cancer cells. The schematic of the dual-modified nanostructured lipid carrier (NLC) system modified with TMSP and folate is shown in Fig. 1. The TMSP includes three units: the cell-penetrating domain (oligoarginine, r9), the MMP-2/9-sensitive cleavable peptide (PVGLIG) and the polyanionic inhibitory peptide (EGGEGGEGG) [14]. r9 is a well-known cell-penetrating peptide (CPP) that enhances the delivery of molecules across biological barriers to achieve intracellular access [22]. TMSP enhances specific cellular uptake through r9 by selectively unmasking of the polyanionic inhibitory peptides in tumor tissue where MMP-2/9 proteases are over-secreted. In circulation, the penetration effect is shielded, but upon arriving at the tumor site, the cleavage of the TMSP is triggered, causing the nonfunctional TMSP to be converted to an activated CPP. The dual-modified design is intended to improve the selective delivery to cancer cells and to reduce intrinsic toxicity to healthy cells beyond the reliance upon the EPR effect and monotarget modification. Simultaneously, CPP penetration, which becomes active after cleavage in the tumor microenvironment with abundant proteases, can overcome the higher interstitial pressure in tumors.

2. Materials and methods

2.1. Materials

Docetaxel (DTX) was purchased from Norzer Pharmaceutical Co., Ltd. Taxotere® was provided by the National Cancer Center. Folate and N,N′-dicyclohexylcarbodiimide (DCC) were obtained from Sinopharm Group Co., Ltd. N-Hydroxysuccinimide (NHS) was purchased from Advanced Chem. Tech. 1,2-Distearoyl-sn-glycero-3-phosphoethanolamine-N-polyethyleneglycol5000-amine (DSPE-PEG5000-NH2) and DSPE-PEG2000-maleimide (DSPE-PEG2000-Mal) were purchased from NOF Corporation. Trypsin was obtained from Amresco, Inc., and 3-(4,5-dimethylthiazol-2-yl)-2,5-diphenyltetrazolium bromide (MTT), 6-coumarin (COU, purity > 99%) and collagenase IV were purchased from Sigma–Aldrich. 4-Aminophenylmercuric acetate (APMA) was purchased from Merck Co., Ltd. All other chemicals were analytical or high performance liquid chromatography (HPLC) grade. Crodamol GTCC®, Crodamol SS® (produced by Croda) and Solutol® HS 15 (produced by BASF) were kindly donated by Fenglijingqiu Commerce and Trade Co., Ltd. Lipoid S PC (produced by Liquid) was purchased from Libaode Bio-Tech Co., Ltd. GM6001 was purchased from Enzo Life Sciences Inc. TMSP and r9 were custom-synthesized via a standard Fmoc solid-phase peptide synthesis method by ChinaPeptides Co., Ltd. Folate-free RPMI-1640 medium and fetal bovine serum (FBS) were obtained from Gibco. RPMI-1640 medium, modified eagle's medium (MEM), F-12K medium, non-essential amino acids, penicillin and streptomycin were provided by Macgene Co., Ltd. Hoechst 33258 was purchased from Molecular Probes Inc. The in situ cell death detection kit was the products of Nanjing Key GEN Biotech. Co., Ltd.

KB cells (human mouth epidermoid carcinoma cells) were grown in folate-free RPMI-1640 medium. HT-1080 cells (human fibrosarcoma cells) were maintained in MEM with Earle's salts, L-glutamine and non-essential amino acids. A549 cells (human pulmonary adenocarcinoma cells) were cultured in F-12K medium. MCF-7 cells (human breast adenocarcinoma cells) were cultured in RPMI-1640 medium. Each cell culture medium was supplemented with 10% FBS, 100 units/mL penicillin and 100 μg/mL streptomycin. The cultures were maintained at 37 °C, 95% relative humidity and 5% CO2.

Female BALB/c nude mice (18–20 g) were purchased from Vital Laboratory Animal Center (Beijing, China), and the animals were then acclimated at 25 °C and 55% humidity under natural light/dark conditions for 1 week before the study, with free access to standard folate-free food and water (Vital Laboratory Animal Center, Beijing, China). All care and handling of animals were performed with the approval of the Institutional Animal Care and Use Committee at Peking University Health Science Center.

2.2. Synthesis of DSPE-PEG2000-TMSP and DSPE-PEG2000-r9

TMSP or r9 peptides were conjugated with DSPE-PEG2000-MAL (1.2:1 molar ratio) in DMF contained triethylamine (TEA, 5 eq) at room temperature (20–25 °C) for 24 h under vigorous stirring [23]. The reaction mixture was dialyzed (molecular weight cutoff (MWCO) 3.5 kDa) in distilled water for 48 h to remove the DMF and unreacted peptides. The final solution was lyophilized and stored at −20 °C until use. The conjugations were confirmed by determining the molecular weight of the resulting DSPE-PEG2000-TMSP or DSPE-PEG2000-r9 using MALDI-TOF MS.

2.3. Synthesis of DSPE-PEG5000-folate

Folate (100 mg, 0.227 mmol) was dissolved in DMSO, and then 93.5 mg DCC (0.454 mmol) was added. After stirring for 15 min, 21 mg NHS (0.182 mmol) was added to the mixture. The reaction was maintained for 6 h at room temperature. The reaction mixture was centrifuged twice at 10,000 rpm for 30 min. The supernatant was quickly transferred with cold anhydrous diethyl ether and acetone (70:30, v/v) into a beaker. The resulting yellow solid was separated by centrifugation. This wash–centrifugation cycle using cold mixture solvent was repeated twice. After the final washing step, folate-NHS was dried in a vacuum at 50 °C and confirmed by MALDI-TOF MS.

Folate-NHS, DSPE-PEG5000-NH2 and TEA (2:1:5 molar ratio) were codissolved in DMSO at room temperature for 24 h under N2 conditions while avoiding light. The reaction mixture was placed in a vacuum at 60 °C using a diaphragm pump to remove pyridine. After adding distilled water to the reaction mixture dropwise, the reaction mixture was centrifuged twice at 14,000 rpm for 15 min. The supernatant was dialyzed (MWCO 25 kDa) in distilled water for 48 h. The final resulting DSPE-PEG5000-folate was confirmed using MALDI-TOF MS [24].

2.4. Cleavage studies of TMSP

The peptide PVGLIG, which was the cleavable linker in the designed TMSP, was evaluated as a substrate for MMP-2/9. To study the sensitivity of the TMSP cleavage by MMP-2/9, activated collagenase IV (containing MMP-2/9) was added to a TMSP solution at a range of concentrations and incubated at 37 °C [14]. Collagenase IV was activated for 1 h at 37 °C with a 2.5 mM APMA solution. At different time intervals, the reaction mixture was quenched by EDTA solution at a final
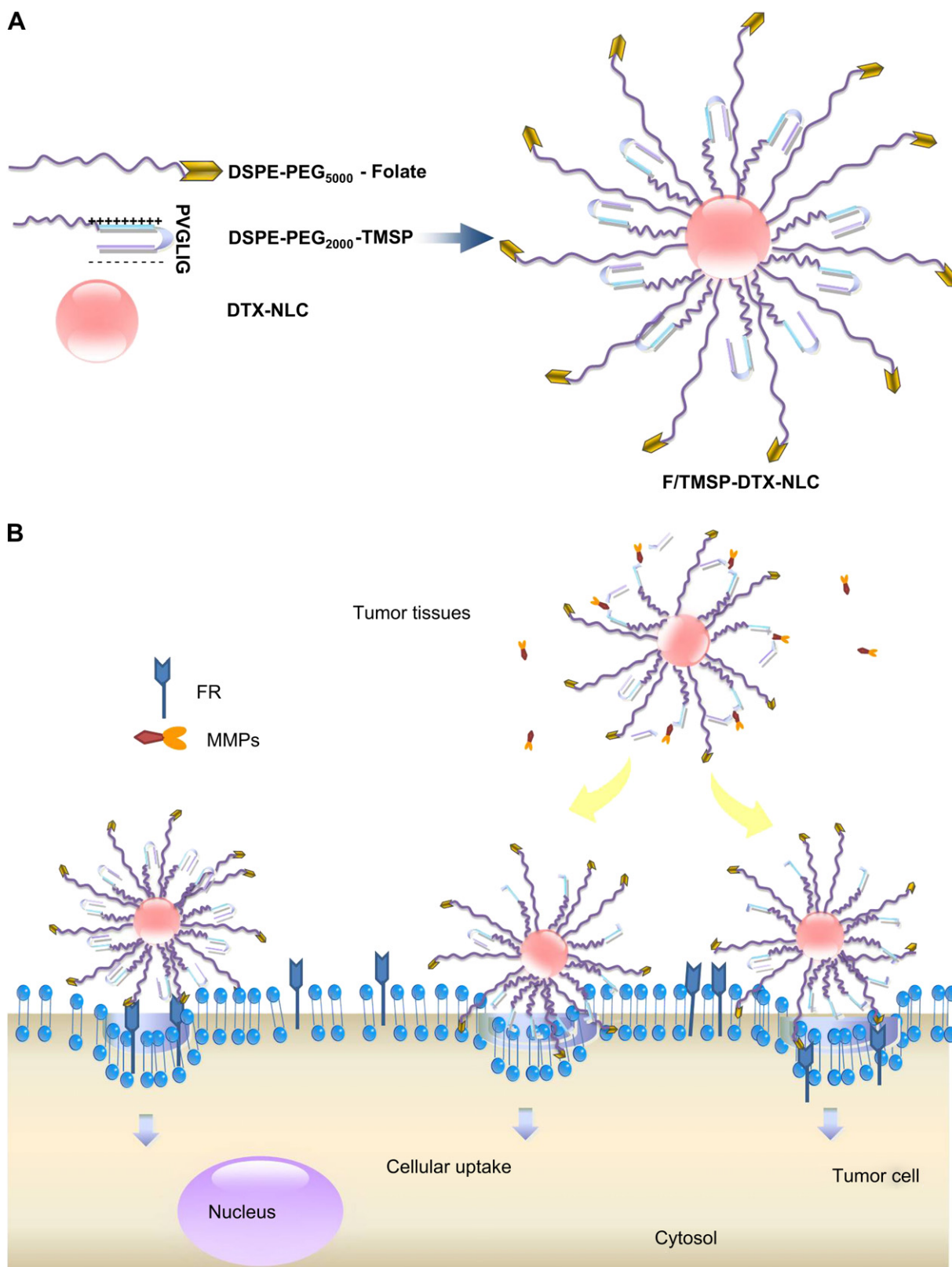
Fig. 1. A schematic of the dual-ligand DTX-NLC simultaneously modified with folate and TMSP (A). The schematic of the multivalent interactions of F/TMSP-DTX-NLC with cancer cells (B).

concentration of 20 mM [25]. TMSP and hydrolyzate were measured by HPLC using a 1525 Pump and Waters 2487 Detector (Milford, MA). The samples were analyzed by HPLC with a mobile phase composed of solvent A (water with 0.1% tri-fluoroaceticacid (TFA)) and solvent B (acetonitrile with 0.1% TFA). The gradient elution was performed as follows: 0–18 min, from 90% solvent A to 50% solvent A; 18–20 min, from 50% solvent A to 10% solvent A. This system was sustained at 100% solvent B for 5 min. The flow rate was 1 mL/min, and the measurement wavelength was 220 nm.

2.5. Preparation of various DTX-NLC

Docetaxel-loaded NLC was prepared by a modified emulsification–ultrasonication method [26]. Docetaxel, Crodamol SS® and Crodamol GTCC® were dissolved in a minute amount of ethanol by heating to 60 °C. The ethanol was removed by magnetic stirring for 20 min. Soya lecithin and Solutol HS15® were dissolved in distilled water to form an aqueous phase and were kept in a water bath at 60 °C. The aqueous phase was added into the melted lipid under magnetic stirring. The obtained primary emulsion was ultrasonicated and cooled until an NLC solidification dispersion was obtained. DTX-NLC was filtered through a 0.22 μm membrane filter. For the preparation of various modified DTX-NLC such as r$_9$-DTX-NLC and F/TMSP-DTX-NLC, an identical procedure was followed except that either only 3% DSPE-PEG-r$_9$ or both 3% molar DSPE-PEG-TMSP and 1% DSPE-PEG-folate were used to replace an equivalent quantity of soya lecithin.

2.6. Physicochemical characteristics of various DTX-NLC

HPLC was used for the quantitative determination of DTX. The HPLC system consisted of a Shimadzu LC-20AT Pump, a Shimadzu SPD-20A UV detector and a SIL-20A autosampler (Shimadzu, Japan). The mobile phase consisted of acetonitrile: double-distilled water (60:40, v/v) introduced at a flow rate of 1 mL/min. The detection wavelength was 230 nm. An RP-18 column (4.6 mm × 250 mm, pore size 5 μm, Diamonsil®) was used.

An ultrafiltration technique was used to separate the unentrapped DTX from DTX-NLCs. A total of 0.5 mL DTX-NLC or targeted DTX-NLC was placed in the upper chamber of a centrifuge tube matched with an ultrafilter (Amicon ultra, Millipore Co. USA, MWCO 10 kDa) and was centrifuged for 30 min at 14,000 rpm at 4 °C. The ultrafiltrate in the ultrafilter containing the unencapsulated DTX was determined by HPLC, as described above. The amount of DTX incorporated into the NLCs was determined through ethanol dilution and ultrasonic disruption by HPLC.

The entrapment efficiency (EE%) and drug loading (DL%) were calculated using the following equations:

$$EE\% = \left[\left(W_{total\ drug} - W_{free\ drug} \right) \big/ W_{total\ drug} \right] \times 100\%$$

$$DL\% = \left[\left(W_{total\ drug} - W_{free\ drug} \right) \big/ W_{total\ lipids} \right] \times 100\%$$

where $W_{total\ drug}$, $W_{free\ drug}$ and $W_{total\ lipids}$ represent the total amount of DTX in the NLCs, the amount of free drug in the ultrafiltrate and the amount of lipid added into the system, respectively.

The mean diameter, particle distribution and zeta potential of these DTX-NLCs were measured by dynamic light scattering using a Malvern Zetasizer Nano ZS (Zetasizer 3000HS, Malvern, Worcestershire, UK) at 25 °C. The DTX-NLC and targeted DTX-NLC were suitably diluted with distilled water to avoid multiscattering phenomena.

These DTX-NLCs were morphologically characterized by a transmission electron microscope (JEOL, JEM-200CX, Japan). The DTX-NLC was diluted with distilled water, and then droplets were deposited on the surface of a Formvar-coated copper grid, followed by a negative staining method using uranyl acetate solution (1%, w/v), and then air-dried overnight at room temperature.

2.7. DTX release from NLC in vitro

Drug release studies were performed using a dialysis technique. The experiments were carried out under sink conditions using phosphate buffer solution (PBS, pH 7.4) containing 0.5% Tween-80 (w/w) as the release medium. In brief, 0.5 mL of DTX-NLC dispersion, Taxotere® or DTX ethanol solution was put into a cellulose acetate dialysis bag (MWCO 8–14 kDa) and immersed in 50 mL release medium, followed by magnetic stirring at 100 rpm and 37 °C using a Thermo mixer comfort (Jiangsu Jintan Medical Instruments Co., Ltd. China). Then, 0.5 mL of sample was taken out from the release medium and replaced with an equal volume of fresh release medium at predetermined intervals. The amount of drug released was evaluated by HPLC after filtration through a 0.22 μm membrane filter. The release studies were carried out in triplicate.

2.8. Cellular uptake studies

The enhancement in cellular uptake offered by the dual-mediated drug delivery system was confirmed using flow cytometry with HT-1080 (over-secreted MMP-2/9) [27,28], KB (high level FR expression) [29], MCF-7 (low level FR expression) [30] and A549 (FR negative) cell lines [31,32]. Cellular uptake was determined with different formulations of fluorescent 6-coumarin (COU) loaded NLC. KB, MCF-7, HT-1080 and A549 cells were seeded in 6-well plates (Corning, NY, USA). After incubating for 24 h, the medium in each well was replaced with fresh cell medium without FBS containing free COU or an equivalent concentration of COU-NLC, r$_9$-COU-NLC and F/TMSP-COU-NLC for 2 h. After incubation, the cells were washed twice with cold PBS (0.1 M, pH 7.4), detached with 0.05% trypsin and washed another three times with cold PBS. Finally, the cells were resuspended in PBS and analyzed by flow

cytometry (Becton Dickinson, San Jose, CA, USA). The autofluorescence of the cells was used as a control.

The cellular uptake mechanisms were studied by determining the influence of the FR and MMP-2/9 on the uptake of the F/TMSP-COU-NLC. KB cells were treated with 1 mM free folate to block FR binding for 1 h. Afterwards, the cells were treated with F/TMSP-COU-NLC.

Collagenase IV containing MMP-2 and MMP-9 was activated by 2.5 mM APMA solution at 37 °C for 2 h [33]. The cells were washed twice with PBS (0.1 M, pH 7.4) and pre-incubated with different concentrations of activated enzyme solutions or 100 mM GM6001, a broad spectrum MMP inhibitor, for 1 h. Then, the medium was discarded and replaced with F/TMSP-COU-NLC [34].

2.9. Cytotoxicity assay

The cytotoxicity of Taxotere®, DTX-NLC and F/TMSP-DTX-NLC against HT-1080, KB, MCF-7 and A549 cells was measured using the MTT assay. The cells were seeded into a 96-well plate at a density of approximate 4000 cells per well. After incubation for 24 h, the cells were treated with the various formulations at a range of concentrations for 72 h. Then, 20 μL MTT (5 mg/mL in PBS) was added to each well. After incubation for 4 h, the medium was removed and replaced with 200 μL DMSO solution to dissolve the formazan. The absorbance of each well was measured by an iMark microplate reader (Bio-Rad Laboratories, Hercules, CA, USA) at a wavelength of 570 nm.

2.10. Penetration and inhibition on three-dimensional multicellular tumor spheroids

We chose the three-dimensional multicellular tumor spheroids system as an in vitro model to better reflect the environment that nanocarriers are likely to encounter in vivo [35–38]. Tumor spheroids were formed with KB or HT-1080 cells using the hanging drop method, as described previously [39]. An agarose solution (2%, w/v) was prepared in serum-free RPMI-1640 by heating at 80 °C for 30 min. Each well of a 48-well culture plate was coated with a thin layer (0.2 mL) of this sterilized solution and filled with 900 mL of culture medium. Twenty microliters of cell suspensions containing 1000 cells were suspended on the lid of a 48-well culture plate. The hanging drop cultures were incubated at 48 h for sufficient sedimentation, and then the resulting cellular aggregates were harvested and transferred into the culture medium to grow for another 2 days. Afterwards, the KB and HT-1080 tumor spheroids were incubated with PBS, blank NLC, Taxotere®, DTX-NLC, F-DTX-NLC, TMSP-DTX-NLC, r$_9$-DTX-NLC and F/TMSP-DTX-NLC respectively. The final concentration of DTX was 2 μg/mL and 5 μg/mL for the KB and HT-1080 tumor spheroids, respectively. Growth inhibition was monitored by measuring the size of the tumor spheroids using an inverted phase microscope (Chongqing Optical & Electrical Instrument, Co., Ltd. Chongqing, China). The major (d_{max}) and minor (d_{min}) diameters of each spheroid were determined, and the spheroid volume was calculated using the following formula: $V = 0.5 \times d_{max} \times d_{min}^2$. The change ratio of the tumor spheroid volumes was calculated with the following formula: $R = (V_i / V_0) \times 100\%$, where V_i is the volume of a tumor spheroid after treatment and V_0 is the volume of the tumor spheroid prior to treatment.

The KB and HT-1080 tumor spheroids were subsequently used to evaluate drug penetration. Briefly, the tumor spheroids were incubated with free COU, COU-NLC, F-COU-NLC, r$_9$-COU-NLC, TMSP-COU-NLC and F/TMSP-COU-NLC, respectively. The tumor spheroids were rinsed with PBS before being transferred to chambered cover slips and then analyzed by confocal microscopy (Leica, Heidelberg, Germany). Z-stack images were obtained by scanning the tumor spheroid step by step. The scanning began from the top of the spheroid to the equatorial plane. Each scanning layer was 9 μm in thickness, and the total scan was 63 μm in depth.

2.11. In vivo antitumor efficacy

The antitumor efficacy in vivo was evaluated in KB tumor-bearing mice. Briefly, the mice were subcutaneously injected in the right flank with 0.2 mL of cell suspension containing 3×10^6 KB cells. The mice were randomly divided into 9 treatment groups (10 mice per group), and the tumors were allowed to grow for 5 days to a volume of 100–200 mm^3. Then, each group of mice was treated every three days by tail vein injection with physiological saline; blank NLC; a 10 mg/kg dose of Taxotere®, DTX-NLC, F-DTX-NLC, TMSP-DTX-NLC, r$_9$-DTX-NLC, F/TMSP-DTX-NLC and a 15 mg/kg dose of F/TMSP-DTX-NLC. The tumor volume was measured every day and calculated based on the equation $(a \times b^2)/2$, where a and b equaled the length and the width of the tumor, respectively. The animals were also weighed every day during the experimental period. After 20 days, the mice were sacrificed, and the tumor tissues were removed, weighed and photographed.

2.12. Apoptosis

The percentage of apoptotic cells in frozen tumor sections was determined by the terminal deoxynucleotide transferase (TdT)-mediated dUTP nick-end labeling (TUNEL) assay. After the isolation of the tumor tissue, apoptosis of tumor cells was detected by the TUNEL assay using an in situ cell death detection kit following the manufacturer's instructions. The samples were analyzed using a laser scanning

confocal microscope. The density of apoptotic cells was evaluated by the apoptotic index (AI), which was defined as follows: AI (%) = 100% × apoptotic cells/total tumor cells.

2.13. Statistical analysis

All data are shown as means ± standard deviation (SD) unless particularly outlined. Student's t test or one-way analyses of variance (ANOVA) were performed in statistical evaluation. A P-value less than 0.05 was considered to be significant, and a P-value less than 0.01 was considered as highly significant.

3. Results and discussion

3.1. Synthesis of DSPE-PEG-TMSP, DSPE-PEG-CPP and DSPE-PEG-folate

DSPE-PEG$_{2000}$-TMSP, DSPE-PEG$_{2000}$-r$_9$ and DSPE-PEG$_{5000}$-folate were synthesized as shown in Fig. 2. Here, DSPE-PEG$_{2000}$-r$_9$ was the cleavage product of DSPE-PEG$_{2000}$-TMSP, which was used to compare the penetration ability before and after activation of DSPE-PEG$_{2000}$-TMSP. The folate was conjugated to the DSPE-PEG$_{5000}$-NH$_2$ via two steps. Successful synthesis was evidenced by the molecular shifts in the MALDI-TOF MS analysis (Fig. 3). The final product was then used for preparing targeted DTX-NLCs in experiments.

3.2. Cleavage of TMSP by MMPs in vitro

The TMSP-specific cleavage and unmasking of the polyanionic inhibitory peptide by MMP-2/9 were confirmed by proteolysis experiments in vitro (Fig. 4). It could be observed that the cleavage of TMSP was obviously related to enzyme concentration. With the MMPs/TMSP ratios increased, the degree of cleavage and the speed ratios improves. When the MMPs/TMSP ratios were 0.196:1, about 50% and 82% of the initial intact TMSP construct was cleaved at 0.5 h and at 4 h exposure, respectively. It was confirmed that the TMSP construct is highly susceptible to MMPs enzymatic lysis and the proteolysis velocity was fast at the beginning. Furthermore, the amount of TMSP did no decrease in the absence of MMPs after 4 h of incubation. It was illustrated that TMSP could be present and stable until it came into contact with MMPs. Therefore, the function of target to cancer cell could be realized in vivo.

3.3. Preparation and characterization of NLC

Nonmodified DTX-NLC and monomodified NLC (r$_9$-DTX-NLC, TMSP-DTX-NLC and F-DTX-NLC), as well as folate and TMSP dual-modified NLC (F/TMSP-DTX-NLC), were prepared by the ultra-sonication method [26]. All of the NLCs tested in this research displayed uniform sizes and shapes, as observed in Fig. 5. The mean particle size, zeta potential, entrapment efficiency and the drug loading of DTX-NLC and targeted DTX-NLC are shown in Table 1. The shapes (Fig. 5A), mean particle size, size distribution (Fig. 5B), entrapment efficiency and drug loading were not significantly different among these nanocarriers. The zeta potential of r$_9$-DTX-NLC exhibited a slightly positive charge approximately 0.67 mV, due to the positively charged arginine in the r$_9$ peptides, whereas the surface charges of the other nanocarriers were approximately −2.9 mV.

3.4. DTX release from NLC in vitro

The DTX release (Fig. 5C) from all NLCs showed a similar pattern, but it was significantly prolonged in comparison to that of DTX solution and Taxotere® (a commercial product of DTX). Our data demonstrated that the sustained release of DTX from these NLCs mainly resulted from the erosion and degradation of the

nanoparticle components (data not shown). The similar physico-chemical characteristics of NLCs allowed us to specifically compare the effects of ligands modification on the NLCs uptake and anti-cancer abilities.
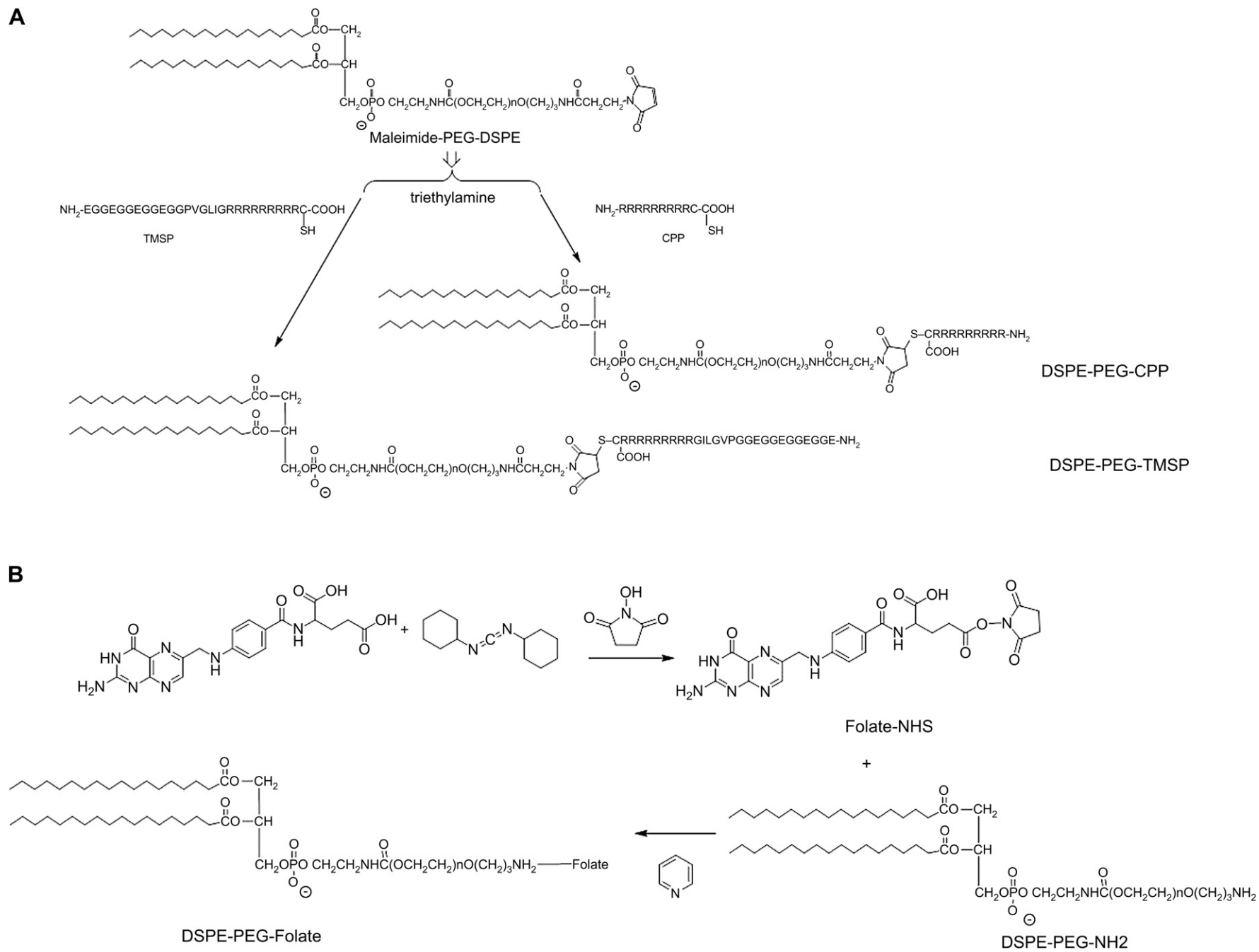
3.5. Selective delivery to cancer cells correspond with FR expression and MMP-2/9 secretion

When TMSP is scissored by MMP-2/9 and activated to r$_9$, the cellular uptake of TMSP-modified NLCs is expected to enhance due to the CPP penetration effect. HT-1080 cells were selected as high MMP-secreting tumor cell type [27,28] to investigate the uptake of TMSP-modified NLCs after MMPs trigger cleavage. After HT-1080 cells treatment with free COU and various COU-loaded NLCs at equivalent concentrations for 2 h, the F/TMSP-COU-NLC demonstrated enhanced cellular uptake ($P < 0.001$) (Fig. 6A). The cellular uptake was also evaluated in the presence of varying concentrations of activated MMP-2/9 which mimicked the increased level of MMPs existing in tumor tissue in vivo, or in the presence of GM6001 (a broad spectrum MMP inhibitor) to exhaust the MMPs [28,40]. F/TMSP-COU-NLC displayed more efficient intracellular delivery with an increasing concentration of MMPs. The intracellular delivery in the presence of 20 μg/mL MMPs was comparable to that of r$_9$-COU-NLC. The intracellular delivery by F/TMSP-COU-NLC was remarkably inhibited upon the addition of GM6001. The sample mean fluorescent intensity declined to a level similar to that of nonmodified COU-NLC. These results demonstrated that the TMSP was available for cleavage by the MMPs in HT-1080 cells becoming r$_9$, which could further enhance cellular uptake.

Based on confirmed reports, KB cells are known to be over-expressed folate receptor [29]. Compared with COU-NLC, F/TMSP-COU-NLC treated KB cells demonstrated much stronger fluorescent intensity ($P < 0.001$, Fig. 6B). Free folate significantly inhibited the cellular uptake of F/TMSP-COU-NLC. These results suggest that FR was strongly involved in the internalization process of dual-modified NLC in KB cells. Interestingly, a slight inhibitory effect on the cellular uptake was found in the presence of GM6001, but a higher fluorescent intensity was found in F/TMSP-COU-NLC treated cells than in r$_9$-COU-NLC treated cells. The maximum cellular uptake was observed for the dual-modified NLC with added activated MMPs. The results predicated that the cleaved dual-modified nanocarriers are taken up by the tumor cells via both receptor-mediated endocytosis and CPP penetrating action.

The cellular uptake of F/TMSP-COU-NLC was increased in MCF-7 cells ($P < 0.01$) but was not obviously increased in A549 cells ($P > 0.05$), compared with that of unmodified COU-NLC (Fig. 6C and D). The results were corresponded with the low level FR expression of MCF-7 cells [30] and negative FR expression of A549 cells [31,32], and revealed the absence of FR resulting reduced internalization. In contrast, F/TMSP-COU-NLC with added activated MMPs and r$_9$-COU-NLC exhibited significantly enhanced cellular uptake in both cell lines. These results demonstrated that TMSP was activatable and that NLC modified with r$_9$ was able to bypass endocytosis and to directly permeate through the cell membrane [41]. The cancer cell recognition by the dual-modifications was greatly enhanced, compared to that of the monoligand and nonmodified NLC.

Overall, these cellular uptake results strongly supported our hypothesis that the multivalent interactions can play a key role in the enhancement of cancer cell recognition and uptake meanwhile the reduction of nonspecific uptake. The folate moiety binds quickly to the FR-positive tumors, and the TMSP moiety is cleaved by MMPs enriched in tumor tissues. The cleaved NLCs (folate and CPP dual-modifications) are then taken up by the tumor cells via either r$_9$'s penetrating activity or receptor-mediated endocytosis (Fig. 1B). These results demonstrated that the enhanced accumulation of the
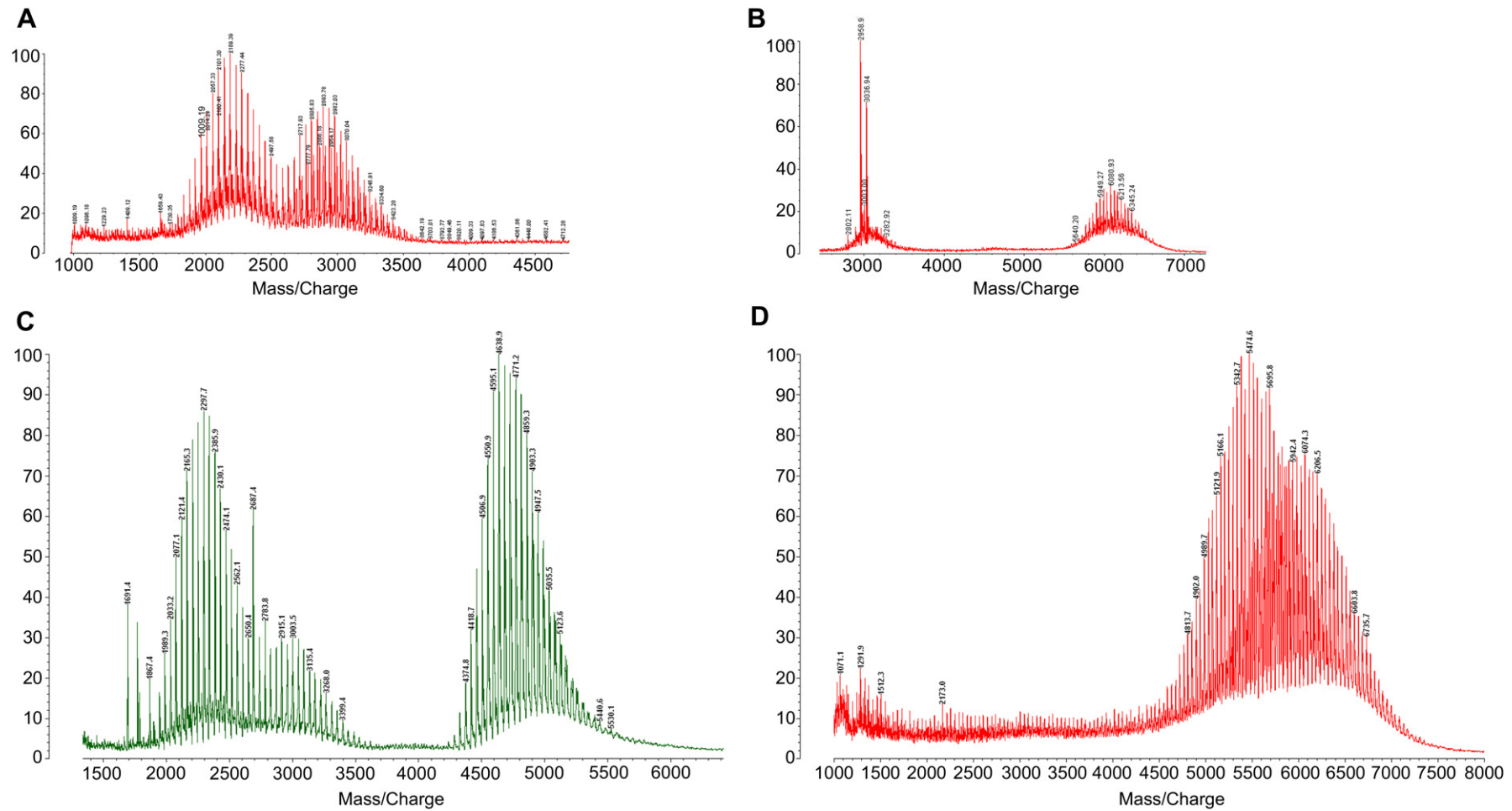
A

Maleimide-PEG-DSPE

NH$_2$-EGGEGGEGGEGGPVGLIGRRRRRRRRRRC-COOH
SH
TMSP

triethylamine

NH$_2$-RRRRRRRRRC-COOH
SH
CPP

DSPE-PEG-CPP

DSPE-PEG-TMSP

B

Folate-NHS

+

DSPE-PEG-NH2

pyridine

DSPE-PEG-Folate

Fig. 2. A schematic representation of TMSP or r$_9$ conjugation with DSPE-PEG$_{2000}$-Mal (A). The synthesis of DSPE-PEG$_{5000}$-NH$_2$ and conjugation with folate (B).

Fig. 3. MALDI-TOF MS spectra of DSPE-PEG$_{2000}$-MAL (A), DSPE-PEG$_{2000}$-TMSP (B), DSPE-PEG$_{2000}$-r$_9$ (C) and DSPE-PEG$_{5000}$-folate (D).
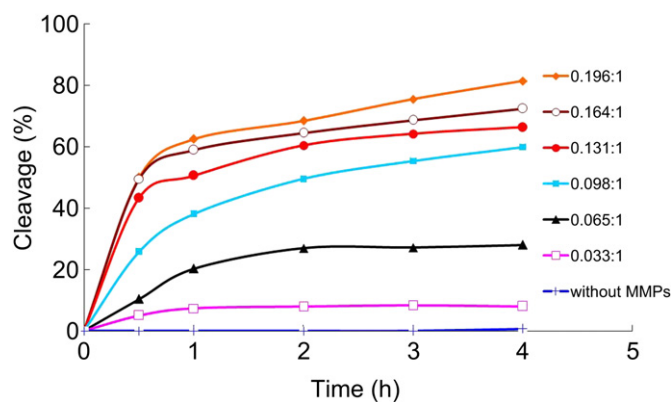
Fig. 4. Cleavage of TMSP by MMPs in different ratios *in vitro*.

dual-modified NLC at the cellular level depends on both TMSP and FR targeting.

3.6. Cytotoxicity

The cytotoxicities of Taxotere®, blank NLC, DTX-NLC and F/TMSP-DTX-NLC were evaluated after incubation with the aforementioned cells for 72 h (Fig. 7). F/TMSP-DTX-NLC exhibited stronger growth inhibition effects on KB and HT-1080 cells, as compared to DTX-NLC, whereas its effects were small on MCF-7 and minimal on A549 cells. These results were consistent with the relative levels of FR expression in the cells. The decrease in cytotoxicity indicated that the high activity in KB-cell killing was attributed to the folate modification after KB cells incubated with free folate for 2 h before treating with F/TMSP-DTX-NLC. It was clear that the selectivity of F/TMSP-DTX-NLC was blocked by free folate. It was noted that KB cells treated with high concentration of DTX-loaded NLC (>100 ng/mL) displayed similar cytotoxicity at both absence and presence of free folate, indicating that competitive block were got over by abundant F/TMSP-DTX-NLC.

F/TMSP-DTX-NLC promoted antiproliferative activities of HT-1080 cells, but the effects remained similar to that of r_9-DTX-NLC. This result appeared to be because the secretion of MMP-2/9 by HT-1080 cells enzymatically cleaved the linker within TMSP to generate r_9 peptides with cell-penetrating action. The effect of cell-penetration may have been as efficient as that of folate targeting in contributing to KB cell cytotoxicity. Additionally, we found that all NLCs demonstrated stronger antiproliferative activities in the four cells than Taxotere®, indicating the enhanced endocytic uptake of NLCs by the tumor cells.

In summary, the cytotoxicity studies demonstrated that the copresentation of folate and TMSP on the modified DTX-NLC promoted antiproliferative activities in cells that overexpressed FR and MMP-2/9. Generally, the results were consistent well with previous cellular uptake studies (Fig. 6) that demonstrated significant and effective enhancement in cellular uptake by the dual-modified drug delivery system. Furthermore, the negligible toxicity of the blank NLC in the four cells confirmed the safety of the nanocarriers.

3.7. Penetration and inhibitory effects on tumor spheroids

The penetration into the three-dimensional multicellular tumor spheroids was determined after applying various NLCs treatment for 12 h (Fig. 8A and B). Free COU and COU-NLC groups did not penetrate into the core of the KB and HT-1080 tumor spheroids. High penetration by r_9-COU-NLC, F/TMSP-COU-NLC and TMSP-COU-NLC, as well as moderate penetration of F-COU-NLC, were observed with KB and HT-1080 tumor spheroids, indicating that the evident penetration was mediated by the r_9 modification and that was temporary masking of r_9 by the polyanionic inhibitory peptide.
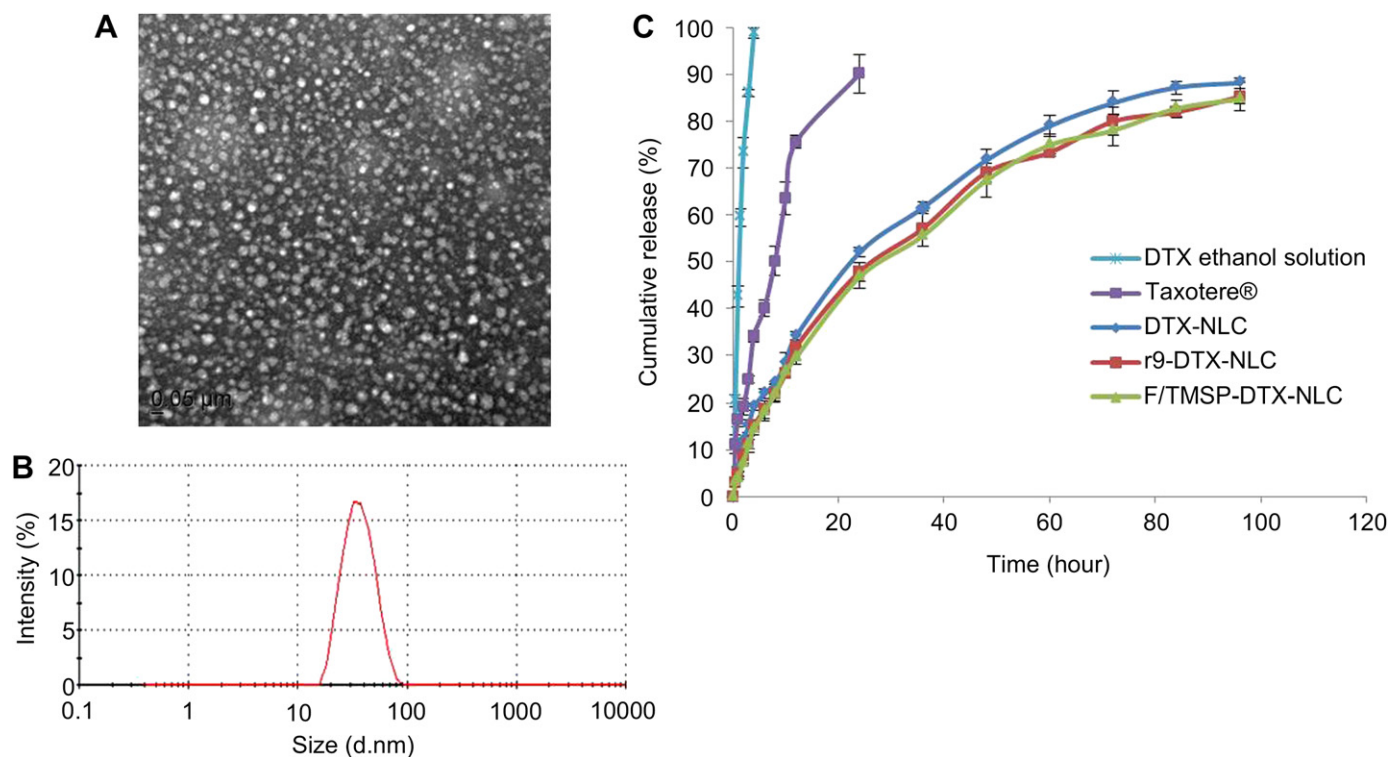

Fig. 5. Transmission electron micrograph of DTX-NLC (A). Scale bar: 50 nm. Particle size distribution of DTX-NLC by dynamic light scattering (B). Docetaxel release profiles from DTX-NLC *in vitro* (C). The data are presented as the mean ± SD (*n* = 3).

Table 1
Characteristics of DTX-NLC.

NLC	Diameter (nm)	Polydispersity index	Zeta potential (mV)	Entrapment efficiency (%)	Drug loading (%)
DTX-NLC	33.17 ± 0.48	0.09 ± 0.01	−2.9 ± 0.70	98.48 ± 0.16	2.40 ± 0.04
F/TMSP-DTX-NLC	35.57 ± 0.31	0.10 ± 0.01	−0.29 ± 0.17	97.47 ± 0.90	2.50 ± 0.04
r9-DTX-NLC	34.17 ± 0.03	0.10 ± 0.01	0.67 ± 0.84	98.49 ± 0.02	2.51 ± 0.06

The data are expressed as the mean ± SD value for at least three different preparations.

Next, the inhibition effect on KB and HT-1080 tumor spheroids growth by various DTX-containing formulations was assessed. Above all, F/TMSP-DTX-NLC produced the most significant reduction in KB and HT-1080 tumor spheroids volume (Fig. 8C and D).

The mono-modified TMSP-DTX-NLC, F-DTX-NLC and r9-DTX-NLC also exhibited a stronger antitumor effect. These results indicated the activity of the targeting and the cell-penetration. Upon binding to the folate ligand, the cancer cells should engulf the nanoparticles
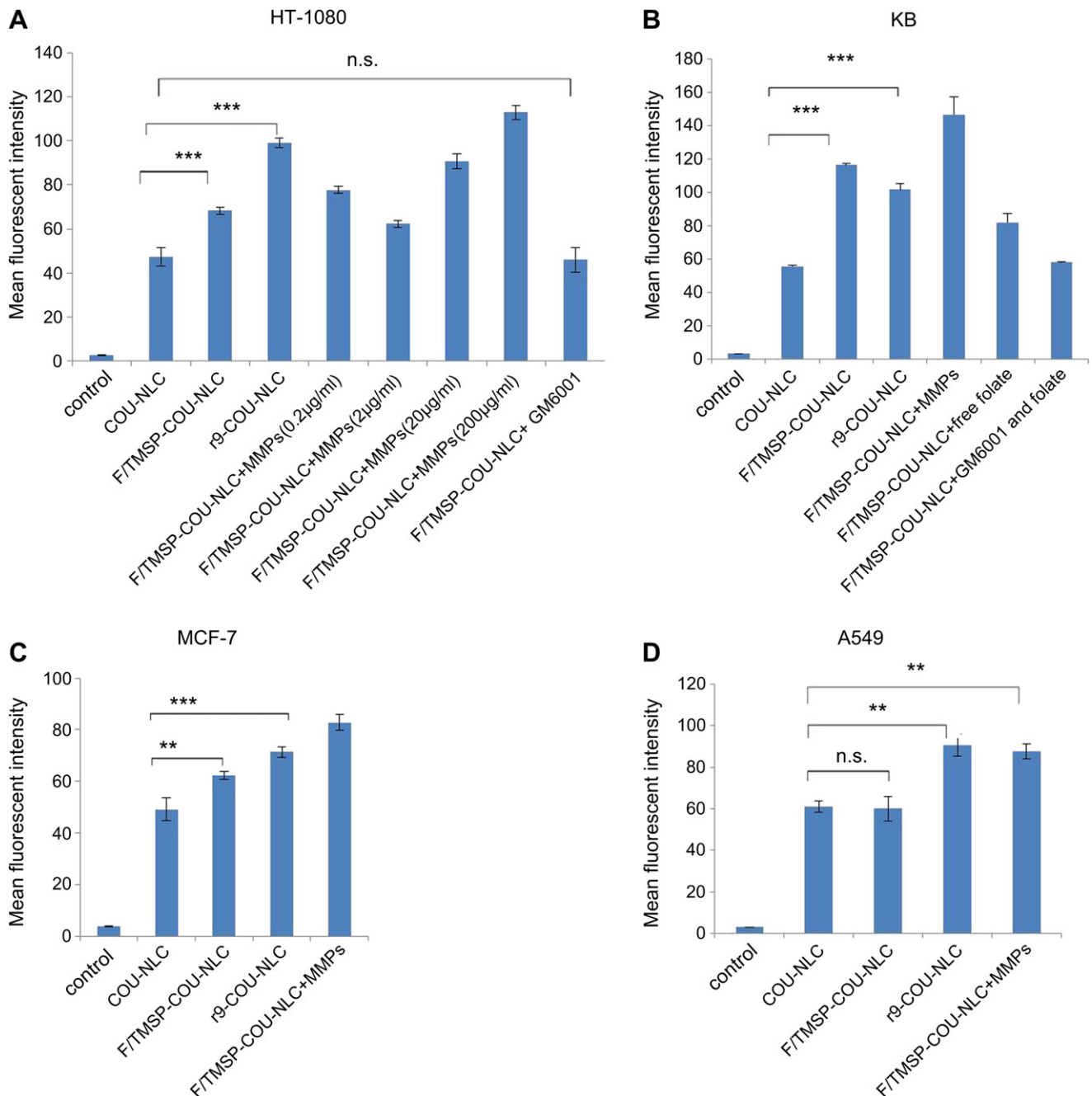

Fig. 6. The cellular uptake in HT-1080 (A), KB (B), MCF-7 (C) and A549 (D) cells after treatment with COU-loaded targeted and nontargeted NLC in the absence and presence of free folate, GM6001 and activated MMPs at different concentrations. The data are presented as the mean ± SD ($n = 3$). *$P < 0.05$; **$P < 0.01$; ***$P < 0.001$; n.s., not significant.
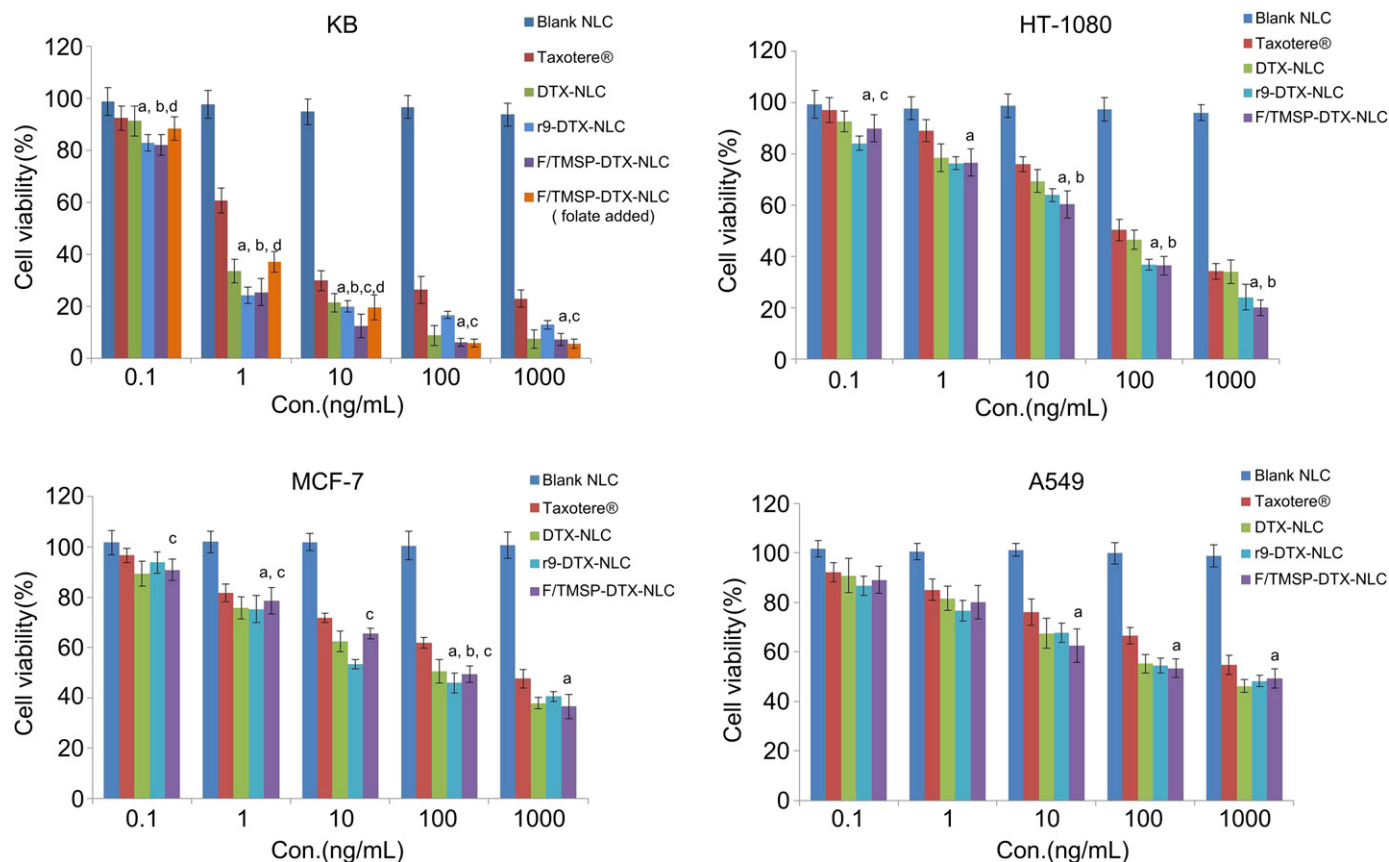
Fig. 7. The viability of KB, HT-1080, MCF-7 and A549 cells cultured with various docetaxel-loaded NLCs in comparison with Taxotere® at the same docetaxel dose and the same amount of blank NLC. The data are presented as the mean ± SD (n = 6). a, $P < 0.05$ versus Taxotere® b, $P < 0.05$ versus DTX-NLC; c, $P < 0.05$ versus r_9-DTX-NLC; d, $P < 0.05$ versus F/TMSP-DTX-NLC blocked by free folate.

by wrapping their cell membranes around the NLC and pinching off an endocytic vesicle inside the cell. In addition, TMSP provides a means of affecting a larger proportion of target cells and enhancing the penetration into tumor spheroids provides to achieve an improved inhibition effect.

3.8. Antitumor activity of dual-modified DTX-NLC

As shown in Fig. 9A, the tumor volume of mice treated with 10 mg/kg doses of DTX-NLC, F-DTX-NLC, TMSP-DTX-NLC, r_9-NLC, F/TMSP-DTX-NLC and 15 mg/kg dose of F/TMSP-DTX-NLC were 2.0-, 4.0-, 2.3-, 2.8-, 6.1-, and 9.6-fold lower, respectively, than those treated with Taxotere® (10 mg/kg) at the end of the study. The tumor growth inhibition by 10 mg/kg doses of Taxotere®, DTX-NLC, F-DTX-NLC, TMSP-DTX-NLC, r_9-DTX-NLC, F/TMSP-DTX-NLC and a 15 mg/kg dose of F/TMSP-DTX-NLC were 88.89%, 92.21%, 96.16%, 94.40%, 95.81%, 98.14% and 98.84%, respectively. The synergistic activity of the folate and TMSP modifications was evident in these results. The excised tumors treated with targeted DTX-NLC exhibited a much smaller weight and size, as shown in Fig. 9C and D. Though poor drug penetration in solid tumors is an intrinsic limitation of chemotherapy that often results in treatment failure [42], the observed antitumor efficacy, as well as the penetration and inhibitory effects on tumor spheroids (Fig. 8) indicates that the dual-modified drug delivery system we designed may be able to solve this problem. The modified NLCs were more effective in reducing the tumor volume, as compared with nontargeted DTX-NLC and Taxotere®.

In respect to safety evaluation, the body weight variation of mice was also monitored during the experimental period (Fig. 9B). There was no significant change of body weight in blank NLC, DTX-NLC, F-DTX-NLC, TMSP-DTX-NLC and F/TMSP-DTX-NLC (10 mg/kg) groups of mice during the whole experimental period. More than 15% of weight loss was found in the F/TMSP-DTX-NLC (15 mg/kg) and Taxotere® (10 mg/kg) groups at the end of experimental period. The weight loss of the Taxotere® group was likely due to the non-targeted characteristics and the toxicity of the formulations' solvent system (ethanol and nonionic surfactant Tween-80) [43]. The inhibitory effects on tumor volume indicated that F/TMSP-DTX-NLC (15 mg/kg) exhibited higher antitumor activity, compared to the 10 mg/kg dose. However, a high drug dose is associated with a higher risk of normal tissue toxicity for cytotoxic drugs. In addition, the smaller of weight loss of mice in F/TMSP-DTX-NLC and TMSP-DTX-NLC groups than that of r_9-DTX-NLC group indicated the TMSP reducing unspecific cellular uptake through shielding r_9 by the polyanionic inhibitory peptides [14]. From these results, it was indicated that the folate- and TMSP-mediated DTX-NLC delivery system was more efficient and safe than Taxotere®, which is more likely due to the selective and efficient cancer cellular uptake.

3.9. Tumor apoptosis analysis

The saline only and blank NLC demonstrated close to no TUNEL positivity, while DTX-treated groups (c–i) exhibited TUNEL positivity (Fig. 9E). The images also revealed that the treatment with DTX-NLC that was modified with folate, TMSP or r_9 could induce
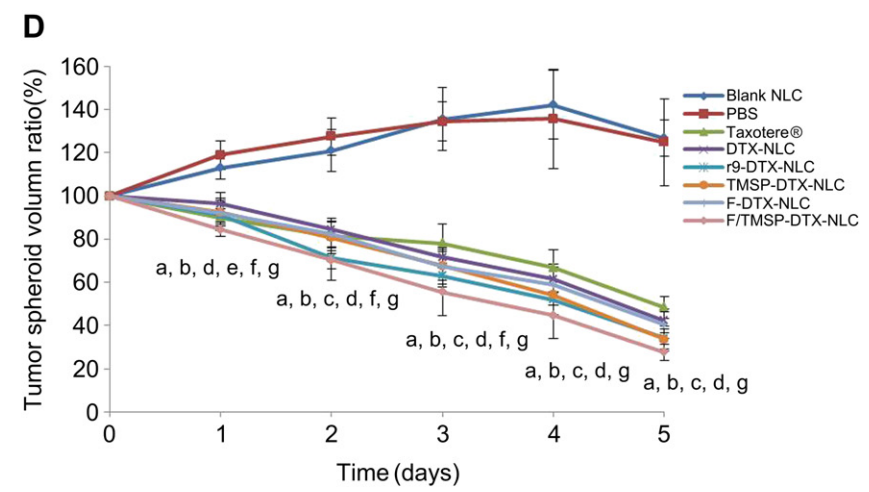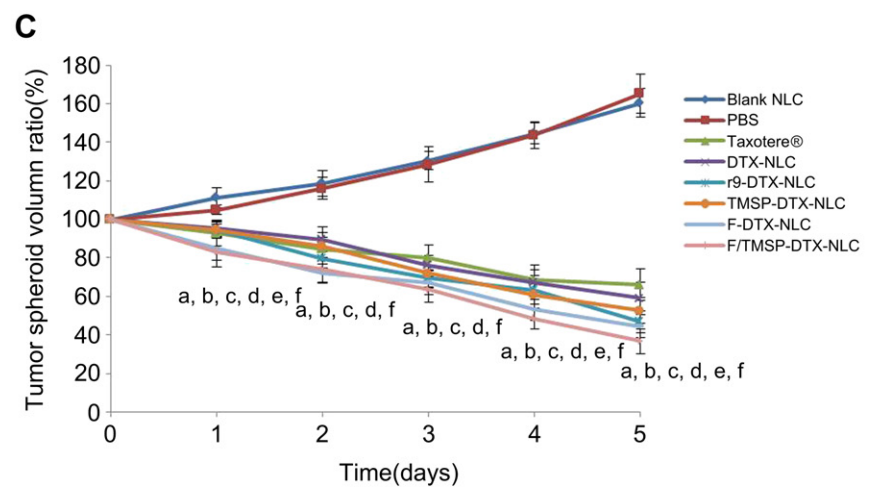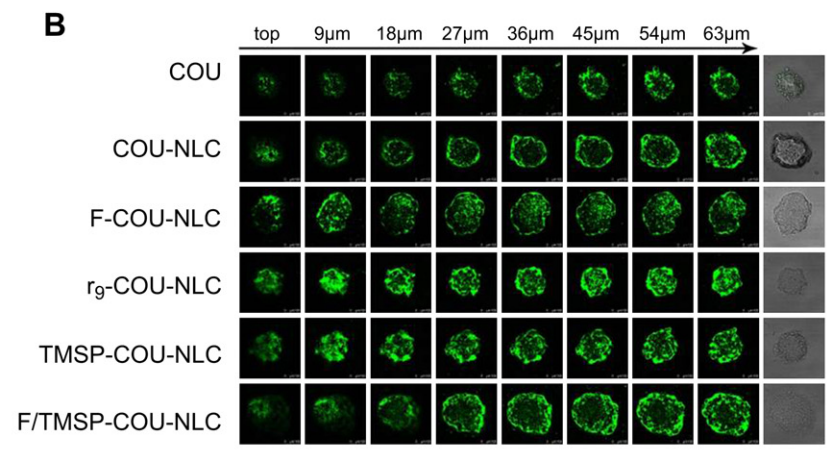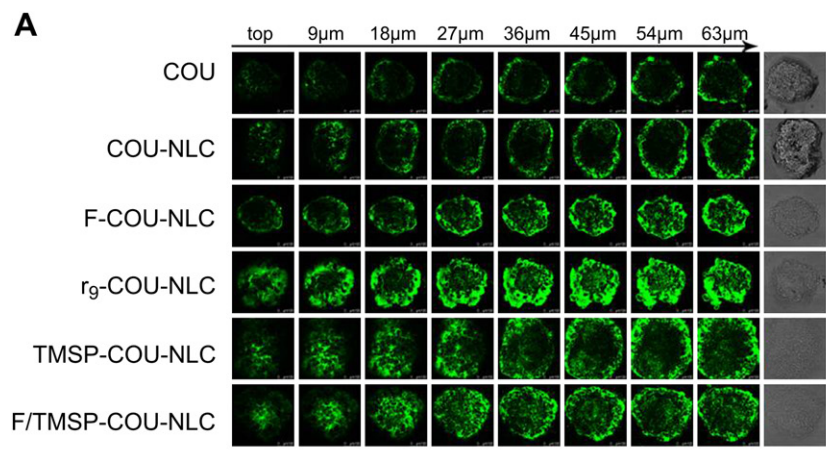
Fig. 8. Confocal images of KB (A) and HT-1080 (B) three-dimensional multicellular tumor spheroids incubated with COU, COU-NLC, F-COU-NLC, r_9-COU-NLC, TMSP-COU-NLC and F/TMSP-COU-NLC for 12 h. Z-stack images were obtained from the top toward the tumor spheroid equatorial plane in 9 μm intervals. The scale bar represents 100 μm. The inhibitory effect on the growth of KB (C) and HT-1080 (D) tumor spheroids after the application of different docetaxel-containing formulations. The data are presented as the mean ± SD ($n = 6$). a, $P < 0.05$ versus blank NLC; b, $P < 0.05$ versus PBS; c, $P < 0.05$ versus Taxotere®; d, $P < 0.05$ versus DTX-NLC; e, $P < 0.05$ versus r_9-DTX-NLC; f, $P < 0.05$ versus TMSP-DTX-NLC; g, $P < 0.05$ versus F-DTX-NLC.
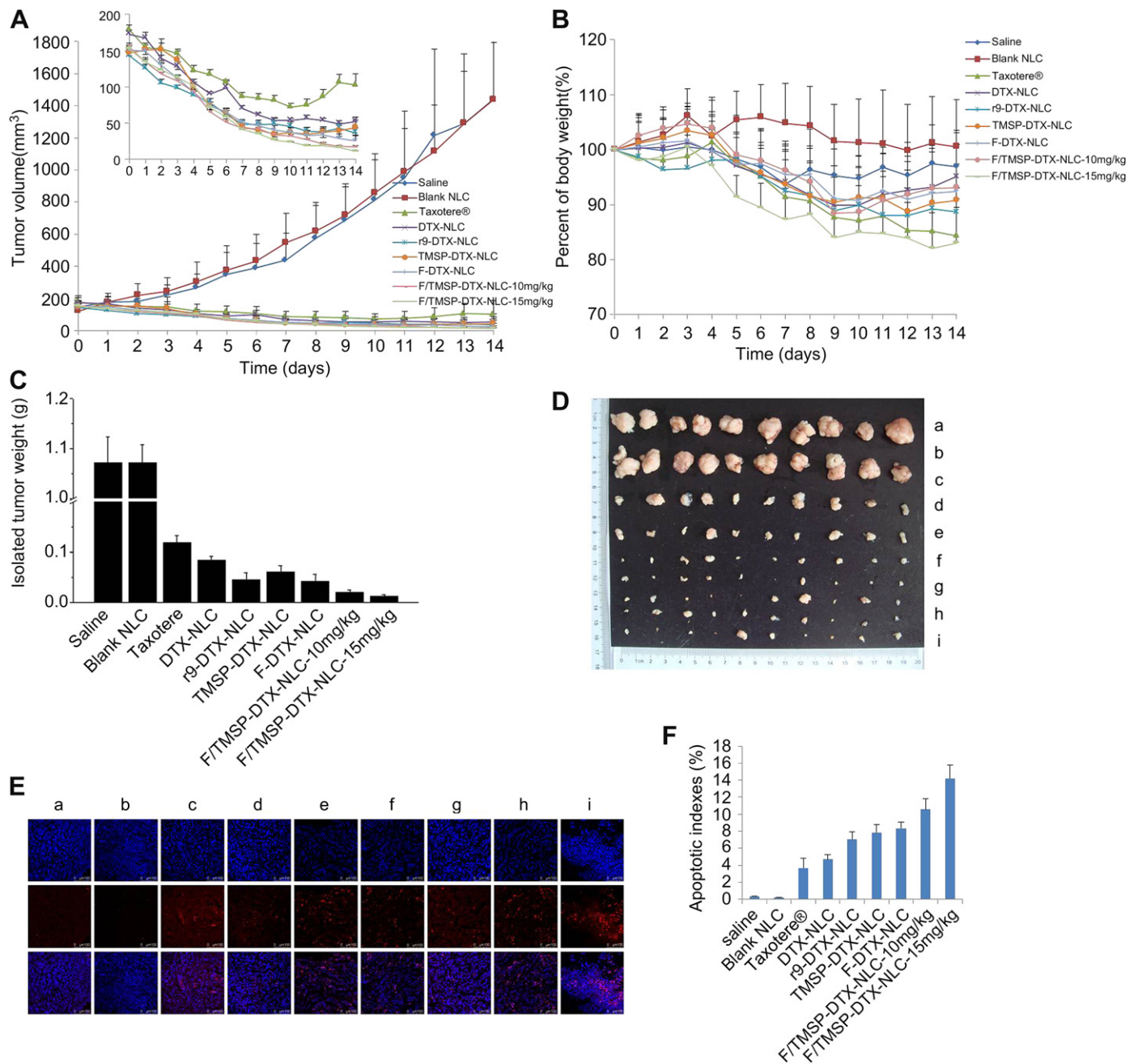
Fig. 9. The *in vivo* antitumor study of docetaxel-loaded NLC in BALB/c mice implanted with KB cells (A). Body weight changes for the tumor-bearing mice (B). The weights of the removed tumors were measured after the completion of the *in vivo* assays (C). The data are presented as the mean ± standard error (*n* = 10). Photograph of the solid tumors removed from different treatment groups at the study termination (D). a: Saline; b: blank NLC; c: Taxotere®; d: DTX-NLC; e: F/TMSP-DTX-NLC; f: F/TMSP-DTX-NLC (15 mg/kg); g: TMSP-DTX-NLC; h: r₉-DTX-NLC; i: F-DTX-NLC. The therapeutic effect on apoptosis by TUNEL staining of the dissected tumor tissue (E). a: Saline; b: blank NLC; c: Taxotere®; d: DTX-NLC; e: F-DTX-NLC; f: r₉-DTX-NLC; g: TMSP-DTX-NLC; h: F/TMSP-DTX-NLC; i: F/TMSP-DTX-NLC (15 mg/kg). The docetaxel treatment dose was 10 mg/kg unless otherwise indicated in the parentheses. The scale bar in E represents 100 μm. Apoptotic cells and cell nuclei were stained by TUNEL (red) and Hoechst 33258 (blue), respectively. Apoptotic indexes for tumors in each group (F). The data are presented as the mean ± standard error (*n* = 3). (For interpretation of the references to color in this figure legend, the reader is referred to the web version of this article.)

the apoptotic death of cancer cells to a greater extent, as compared with treatment with identical doses of the nontargeted DTX-NLC and Taxotere®. Notably, the most apoptotic cells were found in tumor tissues treated with F/TMSP-DTX-NLC (15 mg/kg). Mono-modified (10 mg/kg) TMSP-DTX-NLC, r₉-DTX-NLC and folate-DTX-NLC, as well as the dual-modified F/TMSP-DTX-NLC (10 mg/kg and 15 mg/kg), resulted in a 2.0-, 2.1-, 2.3-, 2.9-, and 3.9-fold increases, respectively, in the apoptotic index, compared with

Taxotere® (Fig. 9F). The trend observed for apoptotic analysis was consistent with the results of the antitumor efficacy *in vivo*.

4. Conclusion

In the present study, we developed a folate and tumor microenvironment-sensitive polypeptides dual-modified doce-taxel-loaded nanostructured lipid carrier (F/TMSP-DTX-NLC). The

nanocarrier system displayed a small size, high encapsulation efficiency (>95%), sustainable release and targeted delivery manner. The enhancement in the cellular uptake and cytotoxic activity of F/TMSP-DTX-NLC in KB, HT-1080, MCF-7 and A549 cells proved the correlation with folate receptor expression and MMP-2/9 secretion. Furthermore, the F/TMSP-DTX-NLC significantly could penetrate deeply into inner of multicellular tumor spheroids due to the function of cell-penetrating peptides. Finally, treatment with F/TMSP-DTX-NLC resulted in stronger antitumor efficacy and enhanced tumor cell apoptosis in KB tumor model in athymic nude mice.

Acknowledgments

References

[1] Immordino ML, Brusa P, Arpicco S, Stella B, Dosio F, Cattel L. Preparation, characterization, cytotoxicity and pharmacokinetics of liposomes containing docetaxel. J Control Release 2003;91:417–29.

[2] Lee E, Kim H, Lee IH, Jon S. In vivo antitumor effects of chitosan-conjugated docetaxel after oral administration. J Control Release 2009;140:79–85.

[3] Cho HJ, Yoon HY, Koo H, Ko SH, Shim JS, Lee JH, et al. Self-assembled nanoparticles based on hyaluronic acid-ceramide (HA-CE) and Pluronic® for tumor-targeted delivery of docetaxel. Biomaterials 2011;32:7181–90.

[4] Lee SW, Yun MH, Jeong SW, In CH, Kim JY, Seo MH, et al. Development of docetaxel-loaded intravenous formulation, Nanoxel-PM™ using polymer-based delivery system. J Control Release 2011;155:262–71.

[5] Kumari A, Yadav SK, Yadav SC. Biodegradable polymeric nanoparticles based drug delivery systems. Colloids Surf B Biointerfaces 2010;75:1–18.

[6] Fang J, Nakamura H, Maeda H. The EPR effect: unique features of tumor blood vessels for drug delivery, factors involved, and limitations and augmentation of the effect. Adv Drug Deliv Rev 2011;63:136–51.

[7] Law B, Tung CH. Proteolysis: a biological process adapted in drug delivery, therapy, and imaging. Bioconjug Chem 2009;20:1683–95.

[8] Timar F, Botyanszki J, Suli-Vargha H, Babo I, Olah J, Pogany G, et al. The antiproliferative action of a melphalan hexapeptide with collagenase-cleavable site. Cancer Chemother Pharmacol 1998;41:292–8.

[9] Kline T, Torgov MY, Mendelsohn BA, Cerveny CG, Senter PD. Novel antitumor prodrugs designed for activation by matrix metalloproteinases-2 and -9. Mol Pharm 2004;1:9–22.

[10] Denmeade SR, Jakobsen CM, Janssen S, Khan SR, Garrett ES, Lilja H, et al. Prostate-specific antigen-activated thapsigargin prodrug as targeted therapy for prostate cancer. J Natl Cancer Inst 2003;95:990–1000.

[11] Kumar SK, Williams SA, Isaacs JT, Denmeade SR, Khan SR. Modulating paclitaxel bioavailability for targeting prostate cancer. Bioorg Med Chem 2007;15:4973–84.

[12] Devy L, de Groot FM, Blacher S, Hajitou A, Beusker PH, Scheeren HW, et al. Plasmin-activated doxorubicin prodrugs containing a spacer reduce tumor growth and angiogenesis without systemic toxicity. FASEB J 2004;18:565–7.

[13] Vartak DG, Gemeinhart RA. Matrix metalloproteases: underutilized targets for drug delivery. J Drug Target 2007;15:1–20.

[14] Shi NQ, Gao W, Xiang B, Qi XR. Enhancing cellular uptake of activable cell-penetrating peptide-doxorubicin conjugate by enzymatic cleavage. Int J Nanomedicine 2012;7:1613–21.

[15] Allen TM. Ligand-targeted therapeutics in anticancer therapy. Nat Rev Cancer 2002;2:750–63.

[16] Sabharanjak S, Mayor S. Folate receptor endocytosis and trafficking. Adv Drug Deliv Rev 2004;56:1099–109.

[17] Leamon CP, Reddy JA. Folate-targeted chemotherapy. Adv Drug Deliv Rev 2004;56:1127–41.

[18] Weitman SD, Lark RH, Coney LR, Fort DW, Frasca V, Zurawski Jr VR, et al. Distribution of the folate receptor GP38 in normal and malignant cell lines and tissues. Cancer Res 1992;52:3396–401.

[19] Jreyssaty C, Shi Q, Wang H, Qiu X, Winnik FM, Zhang X, et al. Efficient nonviral gene therapy using folate-targeted chitosan-DNA nanoparticles in vitro. ISRN Pharm 2012;2012:369270.

[20] Ross JF, Chaudhuri PK, Ratnam M. Differential regulation of folate receptor isoforms in normal and malignant tissues in vivo and in established cell lines. Physiologic and clinical implications. Cancer 1994;73:2432–43.

[21] Lu Y, Low PS. Folate-mediated delivery of macromolecular anticancer therapeutic agents. Adv Drug Deliv Rev 2002;54:675–93.

[22] Wender PA, Mitchell DJ, Pattabiraman K, Pelkey ET, Steinman L, Rothbard JB. The design, synthesis, and evaluation of molecules that enable or enhance cellular uptake: peptoid molecular transporters. Proc Natl Acad Sci U S A 2000;97:13003–8.

[23] Kibria G, Hatakeyama H, Harashima H. A new peptide motif present in the protective antigen of anthrax toxin exerts its efficiency on the cellular uptake of liposomes and applications for a dual-ligand system. Int J Pharm 2011;412:106–14.

[24] Gabizon A, Horowitz AT, Goren D, Tzemach D, Mandelbaum-Shavit F, Qazen MM, et al. Targeting folate receptor with folate linked to extremities of poly(ethylene glycol)-grafted liposomes: in vitro studies. Bioconjug Chem 1999;10:289–98.

[25] Chau Y, Tan FE, Langer R. Synthesis and characterization of dextran-peptide-methotrexate conjugates for tumor targeting via mediation by matrix metalloproteinase II and matrix metalloproteinase IX. Bioconjug Chem 2004;15:931–41.

[26] Zhang P, Ling G, Pan X, Sun J, Zhang T, Pu X, et al. Novel nanostructured lipid-dextran sulfate hybrid carriers overcome tumor multidrug resistance of mitoxantrone hydrochloride. Nanomedicine 2012;8:185–93.

[27] Giambernardi TA, Grant GM, Taylor GP, Hay RJ, Maher VM, McCormick JJ, et al. Overview of matrix metalloproteinase expression in cultured human cells. Matrix Biol 1998;16:483–96.

[28] Chau Y, Padera RF, Dang NM, Langer R. Antitumor efficacy of a novel polymer-peptide-drug conjugate in human tumor xenograft models. Int J Cancer 2006;118:1519–26.

[29] Saul JM, Annapragada AV, Bellamkonda RV. A dual-ligand approach for enhancing targeting selectivity of therapeutic nanocarriers. J Control Release 2006;114:277–87.

[30] Kim SH, Kim JK, Lim SJ, Park JS, Lee MK, Kim CK. Folate-tethered emulsion for the target delivery of retinoids to cancer cells. Eur J Pharm Biopharm 2008;68:618–25.

[31] Canal F, Vicent MJ, Pasut G, Schiavon O. Relevance of folic acid/polymer ratio in targeted PEG-epirubicin conjugates. J Control Release 2010;146:388–99.

[32] Watanabe K, Kaneko M, Maitani Y. Functional coating of liposomes using a folate- polymer conjugate to target folate receptors. Int J Nanomedicine 2012;7:3679–88.

[33] Bawadi HA, Antunes TM, Shih F, Losso JN. In vitro inhibition of the activation of pro-matrix metalloproteinase 1 (Pro-MMP-1) and pro-matrix metalloproteinase 9 (Pro-MMP-9) by rice and soybean Bowman-Birk inhibitors. J Agric Food Chem 2004;52:4730–6.

[34] Aguilera TA, Olson ES, Timmers MM, Jiang T, Tsien RY. Systemic in vivo distribution of activatable cell penetrating peptides is superior to that of cell penetrating peptides. Integr Biol (Camb) 2009;1:371–81.

[35] Carmeliet P, Jain RK. Angiogenesis in cancer and other diseases. Nature 2000;407:249–57.

[36] Haycock JW. 3D cell culture: a review of current approaches and techniques. Methods Mol Biol 2011;695:1–15.

[37] Friedrich J, Ebner R, Kunz-Schughart LA. Experimental anti-tumor therapy in 3-D: spheroids – old hat or new challenge? Int J Radiat Biol 2007;83:849–71.

[38] Kunz-Schughart LA, Freyer JP, Hofstaedter F, Ebner R. The use of 3-D cultures for high-throughput screening: the multicellular spheroid model. J Biomol Screen 2004;9:273–85.

[39] Del Duca D, Werbowetski T, Del Maestro RF. Spheroid preparation from hanging drops: characterization of a model of brain tumor invasion. J Neurooncol 2004;67:295–303.

[40] Roy R, Yang J, Moses MA. Matrix metalloproteinases as novel biomarkers and potential therapeutic targets in human cancer. J Clin Oncol 2009;27:5287–97.

[41] Pearce TR, Shroff K, Kokkoli E. Peptide targeted lipid nanoparticles for anti-cancer drug delivery. Adv Mater 2012;24:3803–22. 710.

[42] Minchinton AI, Tannock IF. Drug penetration in solid tumours. Nat Rev Cancer 2006;6:583–92.

[43] Tong SW, Xiang B, Dong DW, Qi XR. Enhanced antitumor efficacy and decreased toxicity by self-associated docetaxel in phospholipid-based micelles. Int J Pharm 2012;434:413–9.